Atmospheric Environment 57 (2012) 266–277

Contents lists available at SciVerse ScienceDirect

Atmospheric Environment

journal homepage: www.elsevier.com/locate/atmosenv

# Influence of mineral dust transport on the chemical composition and physical properties of the Eastern Mediterranean aerosol

M. Koçak [a], C. Theodosi [b], P. Zarmpas [b], M.J.M. Séguret [c], B. Herut [d], G. Kallos [e], N. Mihalopoulos [b], N. Kubilay [a], M. Nimmo [c,*]

[a] Institute of Marine Sciences, Middle East Technical University, P.O. Box 28, 33731 Erdemli-Mersin, Turkey
[b] Department of Chemistry, University of Crete, Heraklion, Crete, Greece
[c] School of Geography, Earth and Environmental Sciences, University of Plymouth, Plymouth, UK
[d] Israel Oceanographic and Limnological Research, National Institute of Oceanography, Haifa, Israel
[e] University of Athens, School of Physics, University Campus, 15784 Athens, Greece

ARTICLE INFO

*Article history:*
Received 1 July 2011
Received in revised form
22 March 2012
Accepted 2 April 2012

*Keywords:*
Mineral dust
SKIRON
The Middle East deserts
Saharan desert
Eastern Mediterranean

ABSTRACT

Bulk aerosol samples were collected from three different coastal rural sites located around the Eastern Mediterranean, (i) Erdemli (ER), Turkey, (ii) Heraklion (HR), Crete, Greece, and (iii) Tel Shikmona (TS), Israel, during two distinct mineral dust periods (October, 2007 and April, 2008) in order to explore the temporal and geographical variability in the aerosol chemical composition. Samples were analyzed for trace elements (Al, Fe, Mn, Ca, Cr, Zn, Cu, V, Ni, Cd, Pb) and water-soluble ions ($Cl^-$, $NO_3^-$, $SO_4^{2-}$, $C_2O_4^{2-}$, $Na^+$, $NH_4^+$, $K^+$, $Mg^{2+}$ and $Ca^{2+}$). The dust events were categorized on the basis of Al concentrations $>1000$ ng m$^{-3}$, SKIRON dust forecast model and 3-day back trajectories into three groups namely, Middle East, Mixed and Saharan desert. ER and TS were substantially affected by dust events originating from the Middle East, particularly in October, whilst HR was not influenced by dust transport from the Middle East. Higher AOT values were particularly associated with higher Al concentrations. Contrary to the highest Al concentration: 6300 ng m$^{-3}$, TS showed relatively lower AI and AOT. Al concentrations at ER were similar for October and April, whilst OMI-AI and AOT values were ~2 times higher in April. This might be attributed to the weak sensitivity of the TOMS instrument to absorbing aerosols near the ground and optical difference between Middle East and Saharan desert dusts. The lowest enhancement of anthropogenic aerosol species was observed at HR during dust events ($nssSO_4^{2-}/nssCa^{2+} \sim 0.13$). These species were particularly enhanced when mineral dust arrived at sites after passing through populated and industrialized urban areas.



## 1. Introduction

The global radiative forcing due to atmospheric particles is approximately 1.2 W m$^{-2}$, nearly half of the mean global radiative forcing of 2.63 ± 0.26 W m$^{-2}$ as a result of greenhouse gases (IPCC, 2007). A large range of uncertainty has been reported by the IPCC for aerosol forcing estimates due to the poor state of knowledge regarding the sources, distribution and properties of atmospheric aerosols. Radiative properties of mineral dust particles are varied, causing either a warming or cooling depending on their concentration, vertical distribution in the atmospheric column, particle size and mineralogy as well as the albedo and temperature of the underlying surface (Arimoto, 2001; Harrison et al., 2001; Satheesh and Moorthy, 2005).

Mean Aerosol Index (AI) values determined by TOMS (Prospero et al., 2002; Washington et al., 2003) have illustrated the key source regions of mineral dust and the dominance of the Saharan desert. The chemical composition of mineral dust originating from various desert regions (namely, Saharan, Arabian and Chinese) are relatively similar, consisting of approximately 55–60% $SiO_2$ and 10–15% $Al_2O_3$ whilst other oxides (such as $Fe_2O_3$, CaO, MgO, $Na_2O$ and $K_2O$) are slightly more varied being dependent on source location (Goudie and Midddleton, 2001; Usher et al., 2003a, b; Krueger et al., 2004). However, the mineralogy of dust particles is highly variable and reflects the source region. For instance, dust particles originating from the Libyan, Ahaggar-Massif and Chad deserts are characterized by high concentrations of illite (87%)

* Corresponding author.
*E-mail addresses:* m.nimmo@plymouth.ac.uk, mnimmo@plymouth.ac.uk (M. Nimmo).

1352-2310/$ – see front matter © 2012 Published by Elsevier Ltd.
doi:10.1016/j.atmosenv.2012.04.006

while dust particles from the Libyan, Tibesti, Egyptian, Sinai and Negev deserts are characterized by high concentrations of montmorillonite (55%) and kaolinite (30%). The Mediterranean atmosphere is impacted by different pollutant sources via long range transport and its boundary layer is loaded with pollutants emitted from Western and Eastern Europe (Lelieveld et al., 2002). In addition the Mediterranean is bordered on its southern and eastern shores by arid belts that extend from the west coast of North Africa over to the Middle East. A number of studies have been carried out to identify the aerosol chemical composition (e.g. Kubilay and Saydam, 1995; Querol et al., 2004), the influence of dust events on aerosol composition (e.g. Kubilay et al., 2000; Viana et al., 2002) and mineral dust source regions impacting on aerosol levels in the Mediterranean (e.g. Rodriguez et al., 2001; Escudero et al., 2006). Long range transport of dust from North Africa to the eastern Mediterranean occurs predominantly during the spring and is commonly associated with the eastward passage of a frontal low pressure system, whilst dust from sources in the Middle East is more typically transported to the Eastern Mediterranean in the autumn (Kubilay et al., 2000). In contrast, transport from North Africa to the western and central Mediterranean occurs mainly during the summer (Moulin et al., 1998; Escudero et al., 2006).

Ground based lidar/sun photometer and remote sensing observations have also been applied in order to monitor the vertical aerosol structure and properties in the atmosphere over the Mediterranean region (Dulac and Chazette, 2003; Kubilay et al., 2003; Gobbi et al., 2004; Papadimas et al., 2009). The vertical structure of the Mediterranean lower troposphere is complex, with several turbid layers from the surface up to the clean free troposphere. Saharan dust is found between planetary boundary layer aerosols (1.5 km) and cirrus clouds (6 km; Gobbi et al., 2004). Aerosol optical thickness (AOT) and aerosol radiative forcing are among the highest in the world over the Mediterranean region (Kubilay et al., 2003; Barnaba and Gobbi, 2004; Vrekoussis et al., 2005; Papadimas et al., 2009). This is illustrated by the variability in AOT values, with a minimum being observed during winter (below 0.15) and a maximum being observed during summer (above 0.2). Dust distribution in the Mediterranean atmosphere exhibits a South to North gradient, with a spring maximum in the Eastern/Central Mediterranean (AOT, March, April, May period, dust>0.45; Barnaba and Gobbi, 2004).

Thus the Mediterranean is a unique natural laboratory in which to explore the chemical and physical properties of contrasting aerosol populations. In order to explore the temporal and geographical variability in their chemical and physical properties, aerosols in the Eastern Mediterranean atmosphere were simultaneously collected from three coastal rural sites during two distinct dust periods; October 2007 and April 2008. The influence of two distinct dust source areas (Saharan and the Middle East) on the aerosol chemical composition of aerosols above the Mediterranean has been assessed, for the first time, by applying a combination of >1000 ng $m^{-3}$ Al threshold, the SKIRON dust forecast model, back trajectories, AOT and AI (Kubilay et al., 2003, 2005; Barnaba and Gobbi, 2004; Koçak et al., 2004).

## 2. Methodology

Bulk aerosol samples were collected from three different coastal rural sites located around the Eastern Mediterranean (Fig. 1), (i) Erdemli, Turkey (ER, 36°33′54″N and 34°15′18″E), (ii) Heraklion, Crete, Greece (HR, 35°18′29″N and 25°04′48″E) and (iii) Tel Shikmona, Israel (TS, 32°49′34″N and 34°57′24″E). The ER sampling site (IMS-METU, 22 m above sea level and 10 m away from the sea) is surrounded by cultivated land and greenhouses. The city of Mersin is located 45 km to the east of the sampling site with ~800,000 inhabitants. Soda, chromium, fertilizer producing industries and a thermic power plant are located 45 km to the east of the sampling site. The HR sampling site (Voutes campus, UoC, 20 m above ground level, 96 m above sea level and 3.3 km from sea) is surrounded by semi-arid agricultural land. The nearest city is Heraklion located 6 km northeast of the site with a population of 250,000. Industry is not developed in the region, although a power plant is located 6 km north-west of the site. The TS sampling site (22 m above sea level on the roof of the National Institute of Oceanography partly built within the sea) is surrounded by the Shikmona marine reserve. East of the sampling site extends the city of Haifa with 250,000 inhabitants. The city's industrial zone is located 10 km northeast of the sampling site behind Carmel mountain.

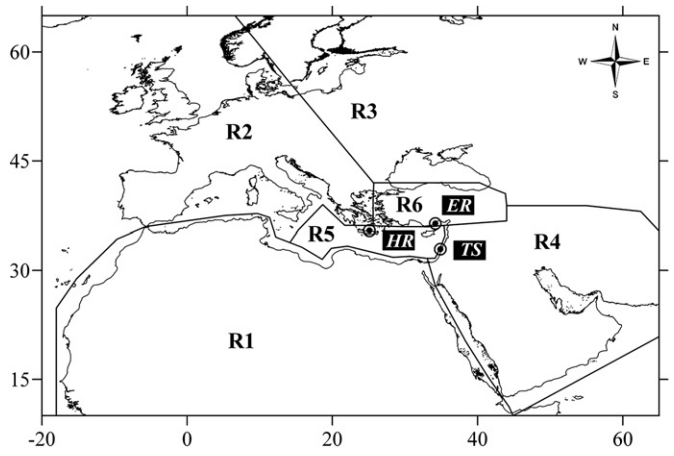


**Fig. 1.** Locations of the sampling sites and classification of 3-day back trajectories arriving at ER, HR and TS. Airflow sectors are presented as R1 (Saharan), R2 (Western Europe), R3 (Eastern Europe), R4 (the Middle East), R5 (Mediterranean Sea) and R6 (Turkey).

The sampling campaigns were carried out during two distinct dust periods; from 7th to 31st October 2007 and from 1st to 30th April 2008. A total of 142 aerosol samples (ER = 54, HR = 48 and TS = 40) were collected using high volume samplers with flow rates of typically 1 $m^3$ $min^{-1}$ on Whatman-41 cellulose fiber filters (20 cm × 25 cm). Mean observational coverage of the sampling period were 89% (% = 54/61 × 100), 79% (% = 48/61 × 100) and 66% (% = 40/61 × 100) at ER, HR and TS respectively. Aerosol samples and blanks obtained from the three sites underwent a total acid digestion (for more details see Seguret et al., 2011). After total dissolution, samples were analyzed for trace elements by Inductively Coupled Plasma Optical Emission Spectroscopy (ICP-OES: Al, Fe, Mn, Ca) and Inductively Coupled Plasma Mass Spectroscopy (ICP-MS: Cr, Zn, Cu, V, Ni, Cd, Pb). The percentage recoveries from certified reference materials (MESS-3, NIST 1648, Estuarine Sediment 1646a, Coal Fly Ash 1633a) for trace elements were >85%, with blank contributions <10% (for details see Seguret et al., 2011). Water-soluble ions ($Cl^-$, $NO_3^-$, $SO_4^{2-}$, $C_2O_4^{2-}$, $Na^+$, $NH_4^+$, $K^+$, $Mg^{2+}$ and $Ca^{2+}$) were measured by ion chromatography (Bardouki et al., 2003). Blank contributions were <5% for all ions. The non-sea salt fractions of $SO_4^{2-}$ and $Ca^{2+}$ were calculated from the $Na^+$ concentration and the standard sea water composition (Turekian, 1976) assuming that the sea salt tracer ($Na^+$) has a pure marine origin. Anthropogenic ($X_{ant} = X_{total} - [(C_R)_{Aerosol} \times (C_X/C_R)_{Reference}]$) fractions of trace elements were estimated from Al and the Saharan end-member composition (for details see Koçak et al., 2007a, b).

Three-day backward trajectories arriving at 1 km above sea level were computed by the HYSPLIT Dispersion Model for each of the sampling sites (HybridSingle Particle Langrangian Integrated Trajectory; Draxler and Rolph, 2003) and illustrated by 1-h

endpoint locations in terms of latitude and longitude. The SKIRON dust forecasting system (Nickovic et al., 2001), the aerosol optical thickness, fine fraction (MODIS; Moderate Resolution Imaging Spectrometer) and aerosol index (AI, OMI; Ozone Monitoring Instrument) were also applied to assess mineral dust transport from desert regions (Herman et al., 1997; Torres et al., 2002; Barnaba and Gobbi, 2004; Kubilay et al., 2003, 2005) and to explore the effect of mineral dust particles on the physical properties of the collected aerosols.

Concentration diagrams (log–log) together with coefficient of divergence, were applied to investigate the similarity between pairs of sampling sites (Wongphatarakul et al., 1998; Zhang and Friedlander, 2000). The log–log diagrams were utilized due to large concentration ranges for aerosol species. The diagonal line represents the hypothetical case where concentrations from each site are equal and divides the concentration diagram into two regions namely, enhanced (above the line) and depleted (below the line). The coefficient of divergence (CD) has been used as a self-normalizing parameter and applied to compare datasets from two different sites (Wongphatarakul et al., 1998; Zhang and Friedlander, 2000). In addition, the *t*-test was used to define statistical differences for each species from all sites after logarithmic transformation.

## 3. Results and discussion

### 3.1. Airflow characterization for October 2007 and April 2008

Airflow climatology has been documented by previous studies for each of the three sites (Mihalopoulos et al., 1997; Koçak et al., 2004, 2005). Back trajectories arriving at ER and TS have, in the past, been divided into six source regions (Koçak et al., 2005). For the current study (see Fig. 1), a similar approach was applied which included the regions R1 (Saharan), R2 (Western Europe), R3 (Eastern Europe), R4 (the Middle East), R5 (Mediterranean Sea) and R6 (Turkey). A summary of the airflow characteristics for each of the three sites expressed as the % influence of airflow from each of the defined six sectors at a 1 km altitude, based on daily air mass back trajectories during October and April, are presented in Table 1. The following general observations can be made:

a) All sites are considerably influenced by Saharan (R1) airflow, especially in April. The % influence of Saharan airflow (R1) in April increases 1.4–2.2 times at the three sites compared with October.
b) ER and TS are substantially affected by airflow from the Middle East (R4), particularly in October, and the airflow from this region exhibits a dramatic decrease (~3 times) at ER and TS from October to April. In contrast, HR is not influenced by airflow from the Middle East during either of these two periods.
c) The % influence of airflow derived from Western Europe exhibits a substantial increase (~2 times) at ER and TS from October to April, whereas the influence of this airflow at HR shows a slight enhancement (1.1 times).
d) The % influence of Eastern Europe (R3) airflow is significant at ER and HR in October. A notable decrease is observed at ER by a factor of 3 from October to April whereas no influence for this airflow is apparent at HR during April. TS is only slightly influenced by airflow from Eastern Europe in October.
e) The influence of airflow from Turkey (R6) is relatively minor at HR (4%) whereas it influences ER (17%) and TS (23%) to a larger extent in October. The percentage influence of Mediterranean (R5) airflow remains relatively steady throughout the sampling periods at HR. Its influence at ER increases from October to April whilst the influence of Mediterranean airflow is opposite to that at TS.

**Table 1**
Summary of airflow characteristics (given as % frequency) at (a) Erdemli (ER), (b) Heraklion (HR) and (c) Tel Shikmona (TS) for six air mass sectors at a 1 km altitude for October 2007 and April 2008.

| Altitude (1 km) | R1 (SAH) | R2 (WE) | R3 (EE) | R4 (ME) | R5 (MS) | R6 (TUR) |
|---|---|---|---|---|---|---|
| (a) ER | | | | | | |
| October | 16.7 | 12.5 | 20.8 | 29.2 | 4.2 | 16.6 |
| April | 36.6 | 30.0 | 6.7 | 10.0 | 10.0 | 6.7 |
| (b) HR | | | | | | |
| October | 40.0 | 36.0 | 16.0 | – | 4.0 | 4.0 |
| April | 54.5 | 40.9 | – | – | 4.6 | – |
| (c) TS | | | | | | |
| October | 22.7 | 13.7 | 4.5 | 18.2 | 18.2 | 22.7 |
| April | 50.0 | 27.8 | – | 5.6 | 5.6 | 11.0 |

Airflow sectors are presented as R1 (SAH, Saharan), R2 (WE, Western Europe), R3 (EE, Eastern Europe), R4 (ME, the Middle East), R5 (MS, Mediterranean Sea) and R6 (TUR, Turkey).

### 3.2. Comparison of aerosol chemical composition in the Eastern Mediterranean

The concentration figures, together with the *t*-test (applied to log-transformed dataset), were used to investigate the similarities in aerosol composition between pairs of sampling sites in the Eastern Mediterranean. Fig. 2 presents the concentrations of elemental species in the collected aerosol samples obtained during October 2007 and April 2008 while Fig. 3 shows the elemental concentration diagrams between pairs of sites.

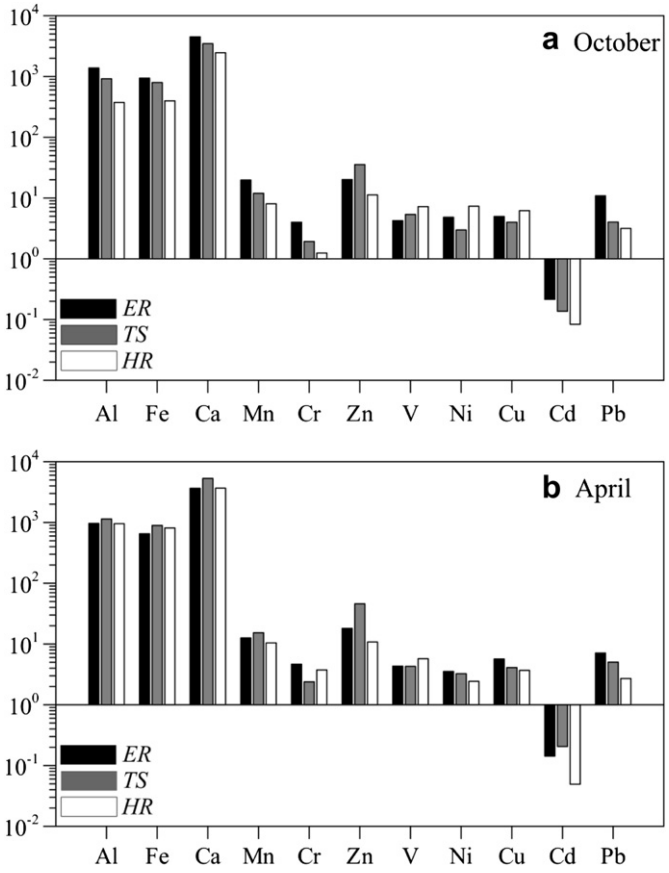


**Fig. 2.** Concentrations of elemental species in bulk aerosol samples obtained during 7–31 October 2007 (a) and 1–30 April 2008 (b). Cr, Zn, V, Ni, Cu, Cd and Pb concentrations are presented as anthropogenic fractions.

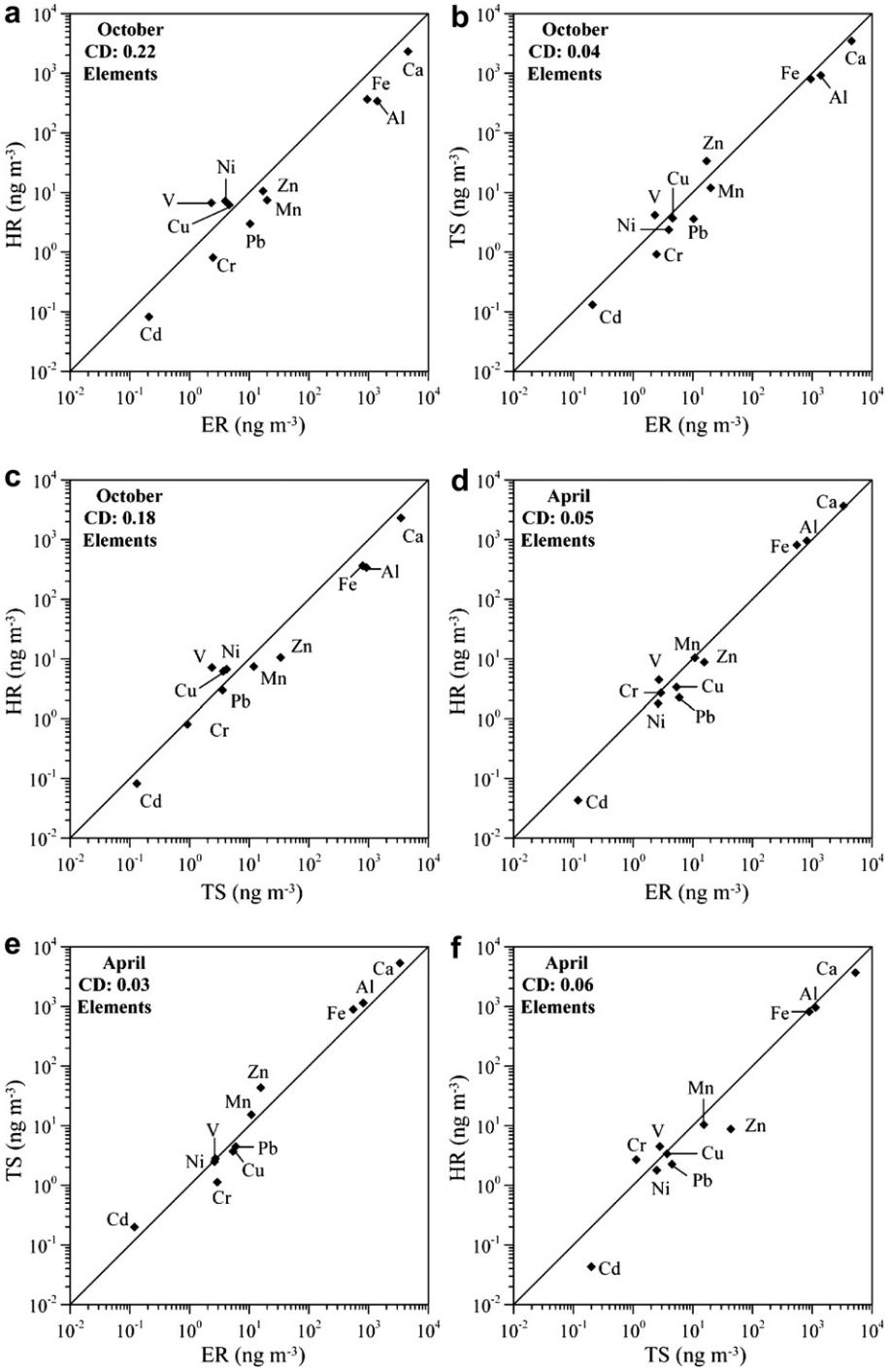


**Fig. 3.** Comparison of elemental concentrations between sampling sites for October 2007 and April 2008. ER vs HR (a), ER vs TS (b), TS vs HR (c), ER vs HR (d), ER vs TS (e) and TS vs HR (f). Cr, Zn, V, Ni, Cu, Cd and Pb concentrations are presented in anthropogenic fractions.

Elemental concentration diagrams for all sites in the Eastern Mediterranean Basin showed strong dissimilarity in October 2007 (Figs. 2a and 3a–c). The results denote that the area extending from the South to North Levantine Basin (TS and ER) have similar elemental aerosol chemical composition whereas, central parts of the Eastern Mediterranean (HR) differs from the two Levantine sites. For instance, crustal elements (Al, Fe, Mn and Ca as well) were 2–4 times higher at ER and TS ($t$-test; $p < 0.01$) than those of HR due to the influence of mineral dust transport, particularly from the desert areas located at the Middle East (see Tables 1 and 2). However, the concentration diagrams comparing elemental composition for April 2008 shows strong similarity (Figs. 2b, 3d–f). This shows considerable spread of the elemental aerosol species area covering the Eastern Mediterranean. Observed differences between October and April may be attributed to the area being affected by the two desert sources: i) the Middle Eastern desert may play a more significant role in the supply of mineral dust over a restricted area of the far Eastern Mediterranean in October ii) during April, mineral dust from the Saharan desert may impact on a larger area over the whole of the Eastern Mediterranean.

**Table 2**
Identified dust events along with possible desert source areas.

| Erdemli (ER) | | | Tel Shikmona (TS) | | | Heraklion (HR) | | |
|---|---|---|---|---|---|---|---|---|
| Date | Case | Possible source | Date | Case | Possible source | Date | Case | Possible source |
| 09-13/10/07 | 1 | ME | 08-09/10/07 | 1 | ME | – | – | – |
| 19-24/10/07 | 2 | ME + SAH | 17-18/10/07 | 2 | ME | – | – | – |
| – | – | – | 26/10/07 | 3 | SAH | – | – | – |
| 30/10/07 | 3 | SAH | 29-31/10/07 | 4 | SAH | 29-31/10/07 | 1 | SAH |
| 06/04/08 | 4 | SAH | 06/04/08 | 5 | SAH | – | – | – |
| 12-16/04/08 | 5 | SAH | 13-17/04/08 | 6 | SAH | 08-14/04/08 | 2 | SAH |
| 21-26/04/08 | 6 | SAH | 23/04/08 | 7 | SAH | 18-23/04/08 | 3 | SAH |

Zn concentrations at TS ($p < 0.01$) were 2–5 times higher than those observed at ER and HR during October and April and this trend has previously been reported (Koçak et al., 2004). This may be attributed to local sources since the largest Zn recycler in the Middle East is located at Maalot, Israel. Enhance Cr aerosol concentrations were observed at ER in October ($p < 0.05$). Elevated concentrations for this element in the region have previously been reported (Kubilay and Saydam, 1995; Güllü et al., 1998; Koçak et al., 2004) and attributed to the presence of ophiolitic rock (enriched in Cr) and extensive Cr ore mining. In addition to the contribution of regionally enriched natural Cr there is also the possibility of aerosol enrichment at ER as a result of anthropogenic derived material. Chromium producing industries are located 45 km to the east of the sampling site. There is also chromium production at Antalya to the west. The Cr industry is very developed in Turkey, being the 8th largest producer in the world. Therefore an anthropogenic derived aerosol Cr component cannot be discounted, and hence may also contribute to the Cr aerosol concentrations observed at ER.

The lowest concentrations of Pb and Cd were observed at HR and the highest V was detected at this site during October and April. Lower Pb and Cd concentrations observed at HR compared to those detected at ER and TS might be attributed to two factors; (i) the far Eastern Mediterranean countries are predominant emitters of Pb and Cd in the region (Pirrone et al., 1999) and (ii) the island sampling site at HR is less influenced from anthropogenic activities than the latter two sites. The higher V values observed at HR may be related to its close proximity to a power plant and shipping emissions (Pandolfi et al., 2010).

Ionic species did indicate statistical ($p < 0.01$) differences between the sites. Sea salt ions ($Na^+$ and $Cl^-$) were found to be higher at TS compared to ER and HR during October. Secondary aerosol species ($nssSO_4^{2-}$, $NO_3^-$, $C_2O_4^{2-}$ and $NH_4^+$) concentrations at HR were 2.1–3.9 time lower than those observed at ER and TS. This might be attributed to i) intense agricultural activities and traffic (particularly for ammonium, sulfate and oxalate), ii) higher contributions from local sources and/or urban agglomerates surrounding the latter two sites (see Table 3) and iii) difference in the photochemical formation which is higher (solar radiation and temperature) at ER and TS compared to HR and thus significant oxidation of adsorbed gaseous precursors onto the dust particles or coagulation between fine particles of these species and mineral dust particles (for more details see Section 3.3.2).

### 3.3. Characterization of dust events in the Eastern Mediterranean

The threshold aerosol Al (proxy for mineral dust) concentration (Al > 1000 ng $m^{-3}$) has been utilized in the Western (Bergametti et al., 1989; Chester et al., 1990; Keyse, 1995) and Eastern (Kubilay and Saydam, 1995; Kubilay et al., 2000, 2005; Koçak et al., 2005) basins in order to identify episodic mineral dust transport over the Mediterranean region. Threshold values should be used with caution since this arbitrary approach may cause misinterpretation during the characterization of dust events. Therefore, for the current study aerosol Al concentrations >1000 ng $m^{-3}$ (as an initial threshold value and indicator), corresponding air mass back trajectories, Aerosol Index and AOT (aerosol optical thickness) obtained from OMI (Ozone Monitoring Instrument), MODIS (Moderate Resolution Imaging Spectrometer) and the SKIRON dust forecasting system were utilized to refine the categorization of mineral dust events at ER, HR and TS during October 2007 and April 2008. Crustal elements show less variability during the summer period owing to the lack of periodic wet precipitation and re-suspension (Güllü et al., 1998; Koçak et al., 2004). Unlike during the summer period, crustal elemental concentrations and their variability are controlled by rain events and dust transport from distant desert source areas during the transitional period (Kubilay and Saydam, 1995). Therefore, for the current study the contribution of re-suspension of local material is expected to be minimal during the transitional period due to a) local rain events (damp soil) and the Ca/Al ratios for dust and non-dust events were distinctly different (see Table 3), the former having a ratio around 2.2–3.3, whilst the latter having a larger ratio of between 4.1 and 7.2.

The daily variations in Al, Fe, Mn and Ca aerosol concentrations at ER, HR and TS along with the corresponding AOT are presented in Fig. 4a, b and c, respectively. Concentrations of these aerosol species obtained from all sites indicate strong daily variability. The corresponding AOT values also denote larger variations during the study period and higher AOT values are particularly found to be associated with higher Al concentrations. Correlation coefficients between Al and AOT were found to be 0.70 for ER, 0.78 for HR and 0.65 for TS.

Table 2 demonstrates the dust events along with possible mineral dust source areas, taking into account the SKIRON dust model simulations and 3-days backward trajectories. Using this approach the dust events were categorized into three groups, Middle East, Mixed and Saharan desert.

#### 3.3.1. October 2007: dust event from the Middle East

The first dust event was characterized from October 9th to 13th (ER: Case 1) and from October 8th to 9th (TS: Case 1) at ER and TS, respectively. The initial signal of this event was observed at TS on October 8th, with an Al concentration of 1400 ng $m^{-3}$ when the airflow was from the Middle East (Fig. 5a). Correspondingly the OMI-AI diagram clearly illustrates a large dust plume over the Middle East on October 8th, between the co-ordinates 18°N–40°N and 35°E–55°E (Fig. 5a), whilst the SKIRON simulated high dust concentrations near ground level, extending from the Israeli coast to Central Iraq (Fig. 5d). The following day, Al values were >2000 ng $m^{-3}$ at ER and TS as a result of the arrival of airflow from the Middle East (Fig. 5b, e). The dust plume intensified and extended over the region particularly between the co-ordinates 30°N–40°N and 35°E–45°E (Fig. 5b, e). On 10th October, the dust cloud disappeared over the Israeli coast (airflow from the Mediterranean Sea). On 11th October, the ER site was still influenced by a dust event (Fig. 5c, f), with the dust activity over the Northern Middle East continuing to affect ER until 13th October.

**Table 3**
Geometric mean concentrations of aerosol species, aerosol index (AI), aerosol optical thickness (AOT) and fine fraction (FF) for dust and non-dust events at Erdemli, Heraklion and Tel Shikmona October 2007 and April 2008.

| Species | Erdemli ($n = 54$) | | | | Heraklion ($n = 48$) | | | | Tel Shikmona ($n = 40$) | | | |
|---|---|---|---|---|---|---|---|---|---|---|---|---|
| | October | | April | | October | | April | | October | | April | |
| | Dust | Non-dust | Dust | Non-dust | Dust | Non-dust | Dust | Non-dust | Dust | Non-dust | Dust | Non-dust |
| Al | 3181 | 599 | 3163 | 328 | 2241 | 293 | 3500 | 201 | 2022 | 547 | 6356 | 299 |
| Fe | 2222 | 396 | 1862 | 246 | 1937 | 320 | 2380 | 224 | 1751 | 532 | 3847 | 208 |
| Ca | 8162 | 2462 | 7024 | 2028 | 7313 | 2121 | 9298 | 1204 | 5527 | 2517 | 13,997 | 1366 |
| Mn | 43.2 | 9.0 | 32.0 | 5.3 | 29.8 | 6.7 | 38.4 | 2.2 | 26.6 | 8.0 | 70.1 | 4.7 |
| Ca/Al | 2.6 | 4.1 | 2.2 | 6.2 | 3.3 | 7.2 | 2.7 | 6.0 | 2.7 | 4.6 | 2.2 | 4.6 |
| Cr[a] | 5.1 | 1.2 | 5.1 | 1.8 | 0.8 | 0.7 | 2.7 | 1.7 | 2.7 | 0.6 | 0.7 | 0.5 |
| Zn[a] | 22.8 | 12.4 | 20.4 | 12.1 | 13.8 | 9.9 | 12.3 | 4.8 | 41.1 | 27.9 | 40.6 | 38.3 |
| V[a] | 6.3 | 0.9 | 5.4 | 1.6 | 10.0 | 6.3 | 5.5 | 2.6 | 7.4 | 3.6 | 6.2 | 1.1 |
| Ni[a] | 7.1 | 2.1 | 4.1 | 1.8 | 7.1 | 6.2 | 2.8 | 0.9 | 4.9 | 1.9 | 5.7 | 1.0 |
| Cu[a] | 4.3 | 4.3 | 5.6 | 4.9 | 7.4 | 5.9 | 4.9 | 1.9 | 6.6 | 3.7 | 6.3 | 1.9 |
| Cd[a] | 0.32 | 0.13 | 0.17 | 0.09 | 0.13 | 0.08 | 0.05 | 0.03 | 0.20 | 0.11 | 0.31 | 0.13 |
| Pb[a] | 15.1 | 6.9 | 8.8 | 4.4 | 4.8 | 2.8 | 2.3 | 1.6 | 5.1 | 3.1 | 8.6 | 2.3 |
| $Na^+$ | 1148 | 1112 | 2044 | 2500 | 1954 | 1941 | 1106 | 1729 | 6418 | 2374 | 3379 | 5089 |
| $Cl^-$ | 1983 | 1854 | 2469 | 3236 | 2301 | 2373 | 2305 | 2691 | 12,585 | 4569 | 7948 | 9193 |
| $Mg^{2+}$ | 423 | 281 | 591 | 369 | 310 | 215 | 407 | 219 | 947 | 501 | 941 | 663 |
| $K^+$ | 486 | 264 | 466 | 322 | 298 | 215 | 198 | 170 | 511 | 362 | 519 | 351 |
| $Ca^{2+}$ | 7085 | 2112 | 6124 | 1761 | 6281 | 1861 | 8264 | 1018 | 4561 | 1774 | 7819 | 1037 |
| $NH_4^+$ | 1707 | 1034 | 1761 | 1537 | 894 | 952 | 260 | 726 | 1020 | 804 | 1121 | 1002 |
| $NO_3^+$ | 6427 | 2701 | 10,869 | 4424 | 5614 | 3657 | 2830 | 2188 | 6604 | 4680 | 10,001 | 3407 |
| $nssSO_4^{2-}$ | 5483 | 2402 | 6991 | 4041 | 5050 | 2750 | 2268 | 1572 | 4093 | 2873 | 6911 | 3153 |
| $C_2O_4^{2-}$ | 474 | 197 | 474 | 223 | 622 | 439 | 140 | 79 | 736 | 519 | 484 | 87 |
| AI | 0.86 | 0.73 | 1.55 | 0.82 | 1.23 | 0.80 | 1.35 | 0.74 | 0.89 | 0.69 | 1.35 | 0.81 |
| AOT | 0.41 | 0.17 | 0.64 | 0.24 | 0.49 | 0.20 | 0.61 | 0.21 | 0.24 | 0.22 | 0.48 | 0.22 |
| FF | 0.38 | 0.45 | 0.15 | 0.28 | 0.35 | 0.54 | 0.20 | 0.28 | 0.23 | 0.27 | 0.13 | 0.33 |

[a] Shows anthropogenic fractions of aerosol trace metals.

### 3.3.2. October 2007: the mixed dust event

A second dust event was observed from 19th to 24th (ER: Case 2) and from 17th to 18th (TS: Case 2) October at ER and TS, respectively. Similar to Case 1, the impact of the dust event was first detected at TS. The OMI satellite image for the 18th October (Fig. 6a) indicated a dust cloud over the Middle East extending from 18°N to 35°N to 35°E–45°E whilst the SKIRON simulation detonated a dust plume between the Israeli coast to Central Iraq (Fig. 6d). During the next two days (on 19th and 20th October, Fig. 6b, e) the dust plume became more intense and extended over the Middle East from the east toward the north. The dust event terminated over the Israeli coast on 21st October whilst remaining over the region covering ER until 22nd October. On 22nd October, the dust cloud almost disappeared over the Middle East, whilst a Saharan dust intrusion was taking place and extending toward the Turkish coast at 18 UTC. The dust plume concentrated and spread over the Turkish and Israeli coastlines during the next 24 h during which the air masses back trajectories originated from North Africa (Fig. 6c, f). Although not discussed in detail, it is worth noting that on 26th October a short and weak dust event was observed at TS (TS: Case 3), with two dust events being observed over the three sites at the end of the October (ER: Case 3, HR: Case 1, TS: Case 4) and around 6th April (ER: Case 4, TS: Case 5). Considering the back trajectories, AI (OMI) and AOT (MODIS) and the dust model (SKIRON) simulations, these events were characterized as Saharan in their origin.

### 3.3.3. April 2008: dust event from Sahara

The last two intense dust outbreaks influencing all three sites were observed after the first week of April. Figs. 7 and 8 highlight the corresponding air mass back trajectories and the OMI satellite image for these events. The air mass back trajectories clearly show airflow at 1 km level reaching all the sampling sites from North Africa. The corresponding OMI satellite images also indicated heavy dust activity over North Africa and the dust cloud covered a significant area extending to the Eastern Mediterranean. Taking into account ground measurements, air masses back trajectories and dust model simulations both dust events were found to be similar in terms of intrusion and spread pattern over the Eastern Mediterranean. For instance, on 17th April at 12 UTC SKIRON simulations demonstrated an intense dust plume, particularly over Libya. During the next 24 h, the dust plume moved toward the northeast and influenced the HR sampling site (Fig. 8a, b). During this period, the Al concentration at HR exceeded 5000 ng $m^{-3}$. In the following 48 h, the dust plume intensified and continued to extend toward the northeast. On 21st, 22nd and 23rd (Fig. 8b, d) April, the dust plume entirely covered the Eastern Mediterranean. The influence of the dust plume appeared to decrease gradually from west to east whilst first ending at HR and then at ER.

## 3.4. Influence of dust events on aerosol chemical composition

### 3.4.1. Aerosol chemical composition

Geometric mean concentrations of aerosol species obtained from October and April for dust and non-dust events for all sites are presented in Table 3. Aerosol species demonstrate distinct differences in chemical composition between dust and non-dust events. For instance, aerosol species originated predominantly from crustal source (Al, Fe, Ca, Mn) were found to be at least four times higher than those observed for non-dust events. Similarly, geometric mean values of anthropogenically derived aerosol trace elements were also found to be enriched during dust events which were 1.1–4.1 times higher than those for non-dust events. Additionally, water-soluble $C_2O_4^{2-}$, $nssSO_4^{2-}$ and $NO_3^-$ indicated enhancements during dust events with values ranging from 1.3 to 5.6. The lowest enrichments were observed at HR.

Geometric means for AI and AOT (550 nm) were 2.9 times higher during dust events. TS exhibited the highest Al concentration with a value of 6300 ng $m^{-3}$ however, observed AI and AOT values were relatively lower than those detected for ER and HR. Al concentrations at ER were similar during October and April, whilst OMI-AI and AOT values in April were ~2 times higher than those observed for October. These observations can be attributed to;

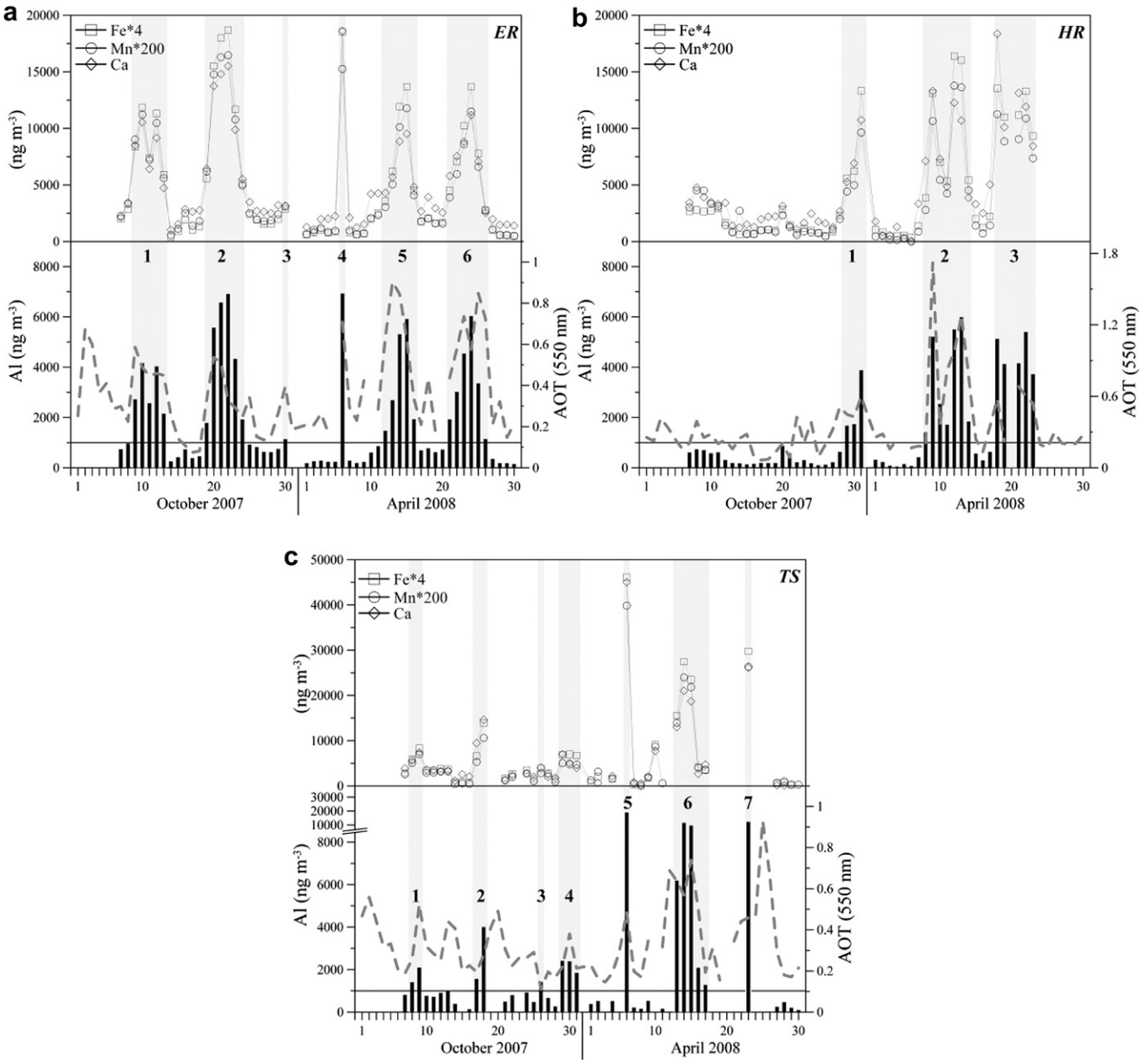


**Fig. 4.** Time series of daily aerosol Al (black bar), Fe (square), Mn (circle) and Ca (triangle) along with $AOT_{550}$ (dashed gray line) at ER (a), HR (b) and TS (c). Solid black line shows the threshold Al value of 1000 ng $m^{-3}$.

a) the weak sensitivity of the TOMS instrument to absorbing aerosols near the ground (Herman et al., 1997; Kubilay et al., 2005), underestimating dust at heights less than 1.5 km and b) optical difference between Middle East originated desert dust and Saharan desert dust, for which the former is identified by a lower AOT (<0.5), higher Angstrom coefficient, higher absorption and an enhanced contribution of the fine fraction (Kubilay et al., 2003). FFs (fine fractions) made lower contributions to the aerosol populations during dust events (about 2 times). The decrease in the fine fraction might be attributed to an increase in the crustal dominated aerosol population which is mainly associated with coarse particles.

### 3.4.2. *Mineral dust as carrier of pollutants*

As is well documented in the literature (Mamane and Gottlieb, 1992; Underwood et al., 2001; Aymoz et al., 2004; Putaud et al., 2004; Koçak et al., 2007a, b), mineral dust particles can serve as reaction surfaces for different aerosol species (including those of anthropogenic origin). Gaseous species such as $SO_2$, $N_2O_5$, $HNO_3$ and $O_3$ can interact with mineral dust. As a result optical properties, size distributions and chemical composition of the atmospheric particles may be altered through these processes during atmospheric transport (Mamane and Gottlieb, 1992; Dentener et al., 1996; Usher et al., 2003a, b). Enhancement of anthropogenic species during dust events might be attributed to several process, including i) anthropogenic species emitted from local sources may mix with mineral dust during air mass transport from desert regions, ii) anthropogenic species may be scavenged with and/or on to mineral dust particle surfaces when air masses from desert areas passes through populated/industrialized regions (Choi et al., 2001; Guo et al., 2004; Vukmirovic et al., 2004).

In order to identify the enrichment of anthropogenic elements and water-soluble ions onto mineral dust particles at the three sites

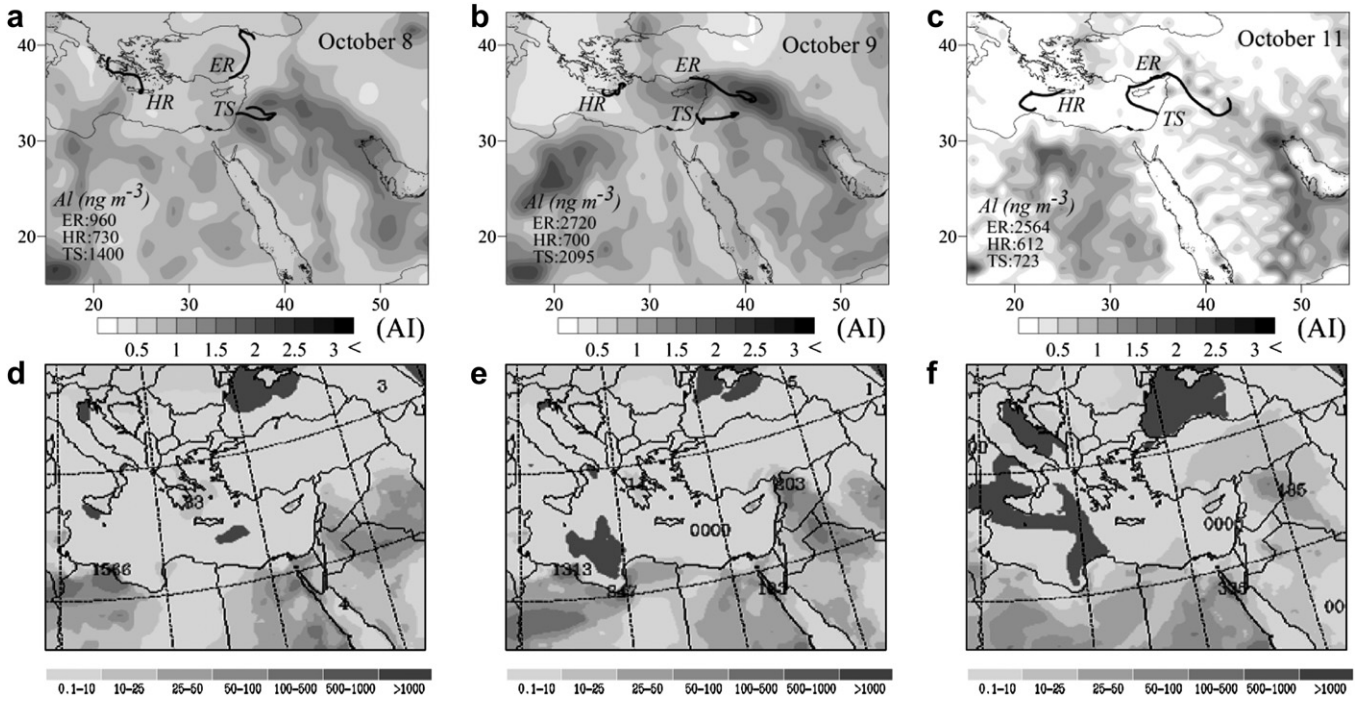


**Fig. 5.** Three day back trajectories and SKIRON dust forecast model illustrating the transport of air masses and dust concentration near ground (μg $m^{-3}$) on 8th of October 2007 (a, d), 9th of October 2007 (b, e) and 11th of October 2007 (c, f). The back trajectory pathway presented by black lines for 1 km. Regional aerosol index from OMI, distribution also presented with a color bar from gray to black.

Al, Pb (non-crustal or anthropogenic fraction), $nssSO_4^{2-}$, $NO_3^-$, $C_2O_4^{2-}$ concentrations and the $nssSO_4^{2-}/nssCa^{2+}$ ratio were considered during the sampling period. The $nssSO_4^{2-}/nssCa^{2+}$ ratio has been applied to assess the Saharan origin of $nssSO_4^{2-}$. For instance, Putaud et al. (2004) suggested Saharan dust is the dominant source of $nssSO_4^{2-}$ in the Western Mediterranean when the $nssSO_4^{2-}/nssCa^{2+}$ ratio is 0.4 ± 0.1. However, lower ratios (~0.3) have been reported over the Eastern Mediterranean (Koçak et al., 2007a, b). Therefore, 0.3 will be used, in the current study, to assess the mineral dust source of $nssSO_4^{2-}$. The lowest $nssSO_4^{2-}/nssCa^{2+}$ ratio with a value of 0.13 was observed at HR on April 2nd during a dust episode. To our knowledge, this is the lowest ratio reported in the

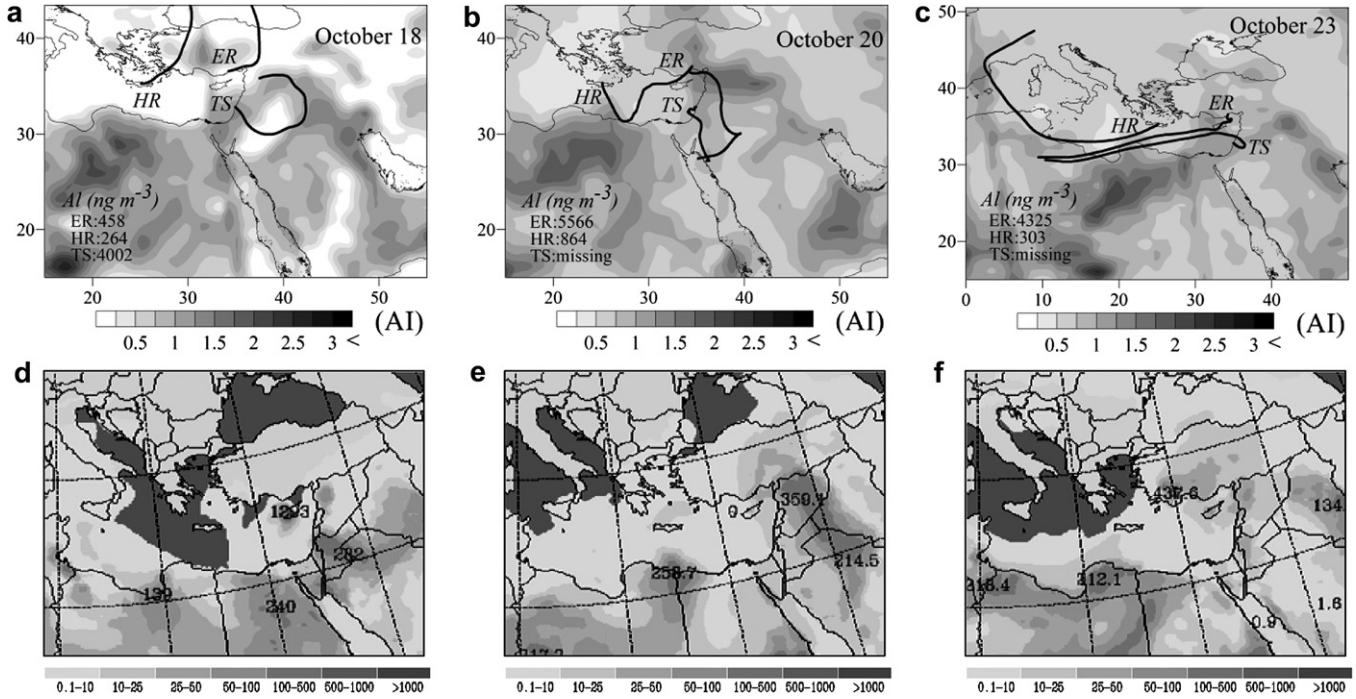


**Fig. 6.** Three day back trajectories and SKIRON dust forecast model illustrating the transport of air masses and dust concentration near ground (μg $m^{-3}$) on 18th of October 2007 (a, d), 20th of October 2007 (b, e) and 23rd of October 2007 (c, f). The back trajectory pathway presented by black lines for 1 km. Regional aerosol index from OMI, distribution also presented with a color bar from gray to black.

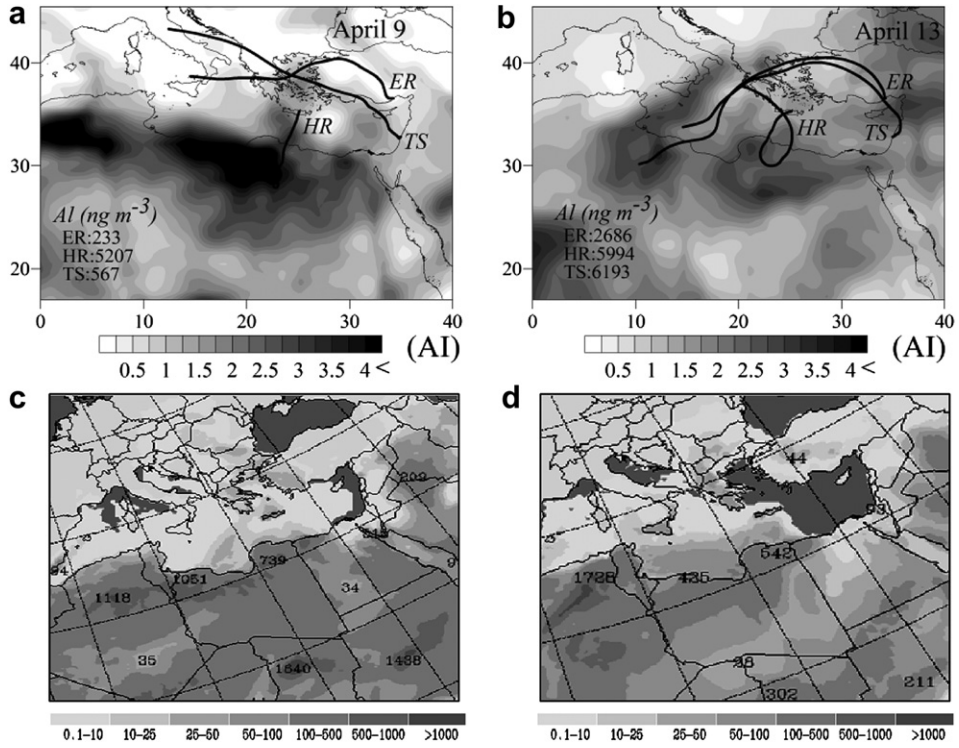


**Fig. 7.** Three day back trajectories and SKIRON dust forecast model illustrating the transport of air masses and dust concentration near ground (μg $m^{-3}$) on 9th of April 2008 (a, c) and 13th of April 2008 (b, d). The back trajectory pathway presented by black lines for 1 km. Regional aerosol index from OMI, distribution also presented with a color bar from gray to black.

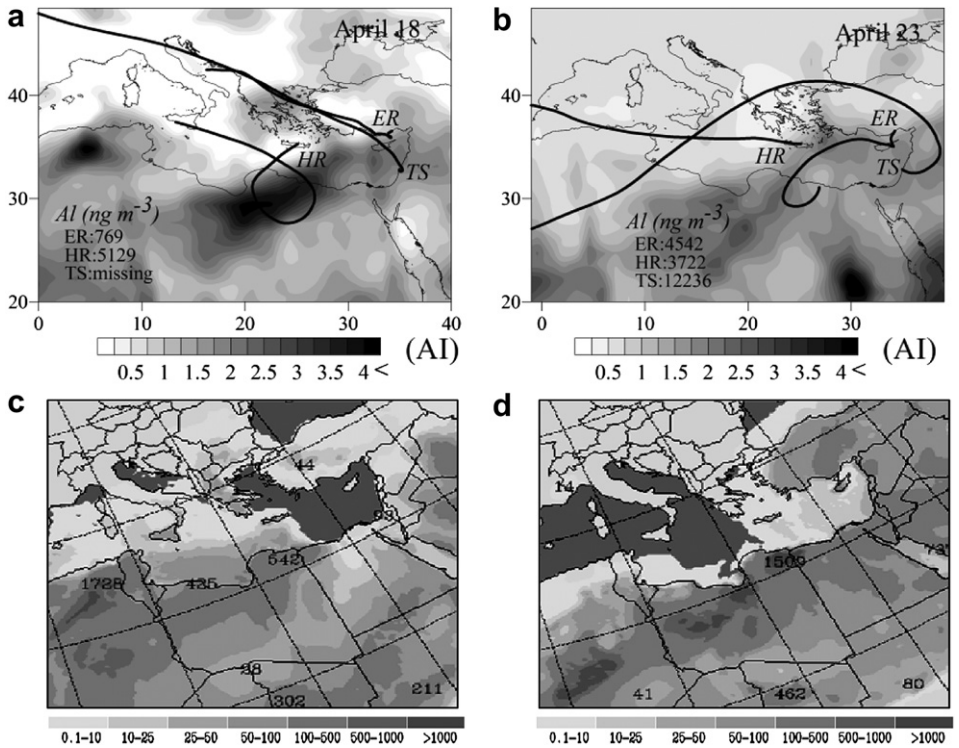


**Fig. 8.** Three day back trajectories and SKIRON dust forecast model illustrating the transport of air masses and dust concentration near ground (μg $m^{-3}$) on 18th of April 2008 (a, c) and 23rd of April 2008 (b, d). The back trajectory pathway presented by black lines for 1 km. Regional aerosol index from OMI, distribution also presented with a color bar from gray to black.

region which shows minimal interaction between sulfate and mineral dust (Putaud et al., 2004; Aymoz et al., 2004; Koçak et al., 2007a, b) for this event.

The lowest enhancement of ant-Pb, $nssSO_4^{2-}$, $NO_3^-$ and $C_2O_4^{2-}$ was observed in aerosols collected from HR compared to those collected from ER and TS during dust events (Fig. 9a, b and c). However, in general concentrations of these species show a gradual increase and a peak during dust events. This is clearly seen in the two case studies with dust events influencing all sites and discussed in details below.

*October 2007*: A marked increase in the concentrations of ant-Pb, $nssSO_4^{2-}$, $NO_3^-$ and $C_2O_4^{2-}$ was observed at ER and at TS during the period of 9th-13th October (ER: Case 1) and 8th -9th October (TS: Case 1), respectively. Concentrations were found to be 1.4–2.5 times higher during dust episodes prior to just before the dust events. For these events, the ratios of $nssSO_4^{2-}/nssCa^{2+}$ were much higher than 0.3 ± 1 (Putaud et al., 2004), ranging from 0.81 to 1.62 at ER (1.43–2.15 at TS). During the dust episode between 29th and 31st October (HR: Case 1) at HR; (TS: Case 4) the corresponding $nssSO_4^{2-}/nssCa^{2+}$ ratios were found to range between 0.34–1.45 and 0.37–1.56 respectively.

In addition the comparative air mass back trajectories reaching ER and HR at a 1 km altitude for the periods between 9th–13th and 29th–31st October 2007 are presented in Fig. 10a. Trajectory analyses show that ER is influenced by dust transport from the Middle East and mineral dust arriving at the site after passing through populated and industrialized regions located to the east of ER. Back trajectories also show transport of the dust over HR after having crossed Italy and Greece (particularly Athens) during the first two days of the dust event, whereas dust transported directly

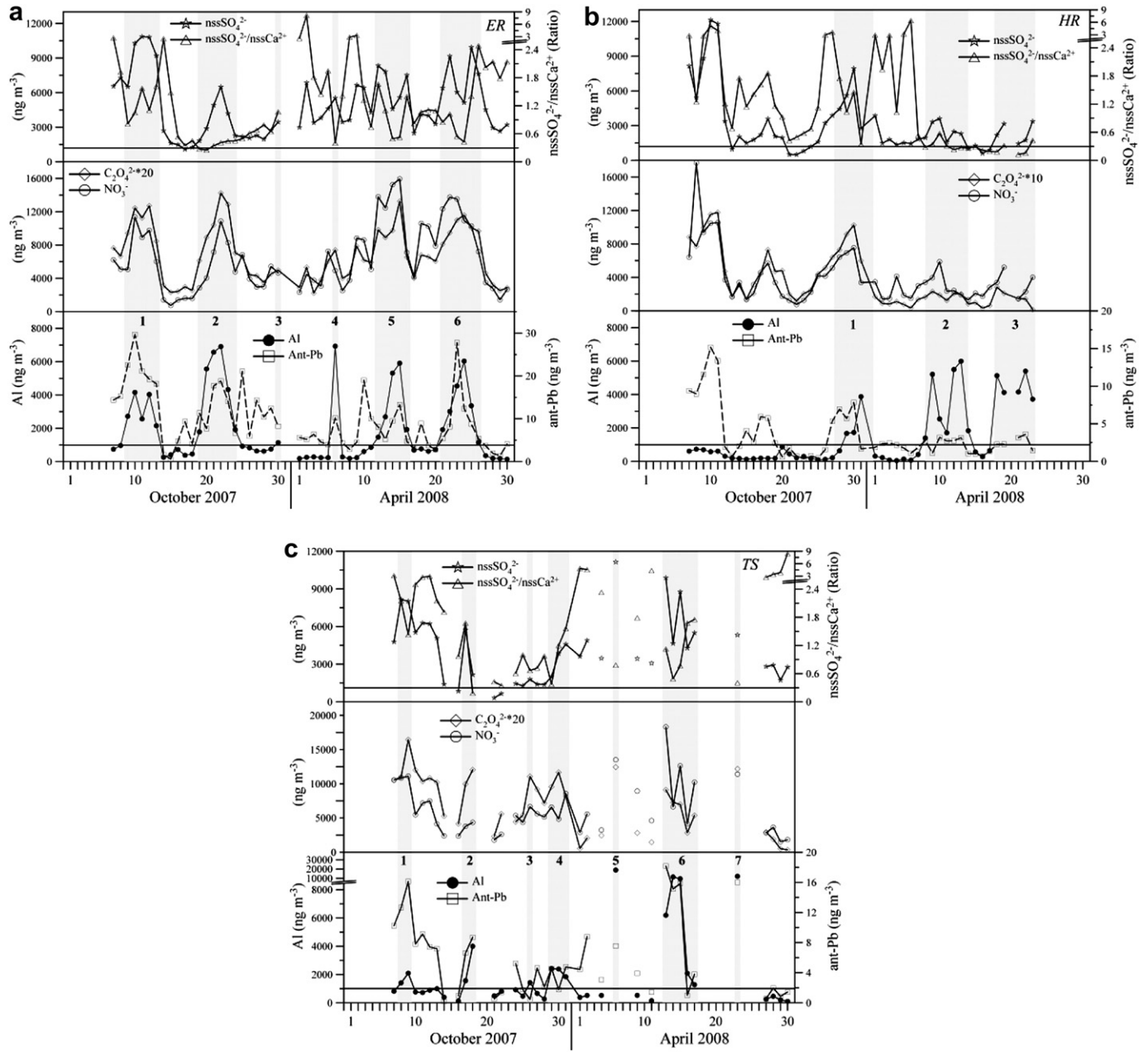


**Fig. 9.** Time series of daily aerosol Al (black circle), ant-Pb (open square), $NO_3^-$ (open circle) and $C_2O_4^{2-}$ (open diamond) $nssSO_4^{2-}$ (open star) along with $nssSO_4^{2-}/nssCa^{2+}$ ratio (open triangle) at ER (a), HR (b) and TS (c). Solid black lines show the threshold Al value of 1000 ng $m^{-3}$ and $nssSO_4^{2-}/nssCa^{2+}$ ratio of 0.3.

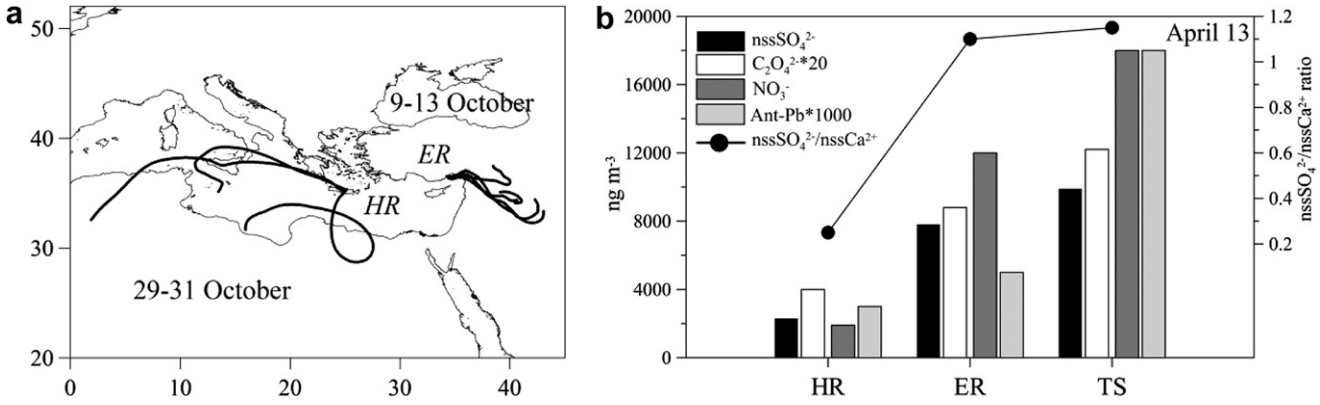


**Fig. 10.** Three day back trajectories illustrating the transport of air masses (black line) between 9 and 13 October 2007 for Erdemli and between 29 and 31 October 2007 for Heraklion (a) and ant-Pb (light gray bar), $NO_3^-$ (dark gray bar) and $C_2O_4^{2-}$ (white bar) $nssSO_4^{2-}$ (black bar) along with $nssSO_4^{2-}/nssCa^{2+}$ ratio (black circle) at HR, ER and TS on 13th of April 2008 (b).

from the Libyan desert on 31st October was associated with the lowest concentrations of anthropogenic species and $nssSO_4^{2-}/nssCa^{2+}$ (0.34) for this specific episode.

*April 2008*: At HR, from 8th to 14th April (HR: Case 2), ant-Pb, $nssSO_4^{2-}$ and $NO_3^-$ values did not show a significant enrichment except on the 10th April ($nssSO_4^{2-}/nssCa^{2+} = 0.57$). Concentrations of these species were found to be enhanced for the periods between 12th–16th (ER: Case 5) and 13th–17th (TS: Case 6) April 2008 with $nssSO_4^{2-}/nssCa^{2+}$ ratios ranging from 0.49 to 1.78, at ER and TS. On 13th April all sites were influenced by mineral dust transport from the Saharan desert (see Fig. 7b,d; particularly from Libya). In this case, trajectories revealed that HR was directly influenced by dust intrusion from the Sahara whereas, mineral dust passed through populated and industrialized sites located in the Balkans and Turkey before arriving at first ER and then TS. The anthropogenic species showed an agreement with this airflow pattern. A clear enrichment was observed for anthropogenic species (see Fig. 10b) in the increasing order of HR (ant-Pb ~ 3, $nssSO_4^{2-}$ ~ 2300, $NO_3^-$ ~ 1900, $C_2O_4^{2-}$ ~ 200 ng $m^{-3}$, $nssSO_4^{2-}/nssCa^{2+}$ ~ 0.25) < ER (ant-Pb ~ 5, $nssSO_4^{2-}$ ~ 7800, $NO_3^-$ ~ 12,000, $C_2O_4^{2-}$ ~ 440 ng $m^{-3}$, $nssSO_4^{2-}/nssCa^{2+}$ ~ 1.10) < TS (ant-Pb ~ 18, $nssSO_4^{2-}$ ~ 9900, $NO_3^-$ ~ 18,000, $C_2O_4^{2-}$ ~ 610 ng $m^{-3}$, $nssSO_4^{2-}/nssCa^{2+}$ ~ 1.15). During the last episodes of the dust events occurring during the periods 20th–26th at ER (on 23 April at TS) and 18th–22nd April at HR, lower enrichment of anthropogenic species were observed at HR compared to the other two sampling sites.

## 4. Conclusion

The temporal and geographical variability in the chemical and physical properties of aerosols in the Eastern Mediterranean atmosphere have been investigated. Simultaneous collection of aerosol samples from three coastal rural sites during two distinct dust periods; October (2007) and April (2008) was carried out. From these findings the following conclusions may be made:

- Crustal elemental (Al, Fe, Mn and Ca as well) concentrations were found to be 2–4 times higher at ER and TS than those observed at HR during October 2007 owing to the influence of mineral dust transport, particularly from the desert areas located in the Middle East. Concentration diagrams comparing elemental composition for April 2008 reveal strong similarity. This distinct difference suggested a) that the Middle East desert may play a significant role in the supply of mineral dust over a restricted area of the far Eastern Mediterranean in October and b) mineral dust from the Saharan desert may impact upon the whole Eastern Mediterranean during April.
- Possible mineral dust source areas were identified by applying a threshold aerosol Al concentration (Al > 1000 ng $m^{-3}$), SKIRON dust model simulations and 3-days backward trajectories. From which, the dust events were categorized into three groups; Middle East, Mixed and Saharan desert. ER and TS were substantially affected by dust events originating from the Middle East, particularly in October, whilst HR was not influenced by dust transport from the Middle East.
- The highest Al concentration was observed at TS with a value of 6300 ng $m^{-3}$, observed AI and AOT values were relatively lower compared to the other sampling sites. Al concentrations at ER were similar during both October and April, whilst OMI-AI and AOT values in April were ~2 times higher than those observed for October. This might be attributed to a) the weak sensitivity of the TOMS instrument to absorbing aerosols near the ground, underestimating dust at heights less than an altitude of 1.5 km and b) optical difference between Middle East desert dusts and Saharan desert dust.
- During dust events concentrations of anthropogenic aerosol species were found to be 1.1–4.1 times higher than those for non-dust events. These species were particularly found to be enhanced when mineral dust arrived at the sites after passing through populated and industrialized urban areas. Although the lowest enhancement of anthropogenic aerosol species was observed at HR during dust events. Indeed, the lowest $nssSO_4^{2-}/nssCa^{2+}$ ratio reported in the region, with a value of 0.13, was observed at HR, indicating minimal interaction between sulfate and mineral dust.

## Acknowledgments

Aerosol optical thickness, fine fraction and aerosol index values used in this study were produced with the Giovanni online data system, developed and maintained by the NASA GES DISC. We also acknowledge the MODIS and OMI mission scientists and associated NASA personnel for the production of the data used in this research effort. This work was supported by NATO (NATO CLG 982862).

## References

Arimoto, R., 2001. Eolian dust and climate: relationships to sources, tropospheric chemistry, transport and deposition. Earth-Science Reviews 54, 29–42.
Aymoz, G., Jaffrezo, J.L., Jacob, V., Colomb, A., George, C., 2004. Evolution of organic and inorganic components of aerosol during a Saharan dust episode observed in the French Alps. Atmospheric Chemistry and Physics 4, 2499–2512.

Bardouki, H., Liakakou, H., Economou, C., Sciare, J., Smolik, J., Zdimal, V., Eleftheriadis, K., Lazaridis, M., Dye, C., Mihalopoulos, N., 2003. Chemical composition of size resolved atmospheric aerosols in the Eastern Mediterranean during summer and winter. Atmospheric Environment 37, 195–208.

Barnaba, F., Gobbi, G.P., 2004. Aerosol seasonal variability over the Mediterranean region and relative impact of maritime, continental and Saharan dust particles over the basin from MODIS data in the year 2001. Atmospheric Chemistry and Physics 4, 2367–2391.

Bergametti, G., Dutot, A.L., Buat-Menard, P., Losno, R., Remoudaki, E., 1989. Seasonal variability of the elemental composition of atmospheric aerosol particles over the northwestern Mediterranean. Tellus 41B, 353–361.

Chester, R., Nimmo, M., Murphy, K.J.T., Nicolas, E., 1990. Atmospheric trace metals transported to the western Mediterranean: data from a station on Cap Ferrat. In: Martin, J.M., Barth, H. (Eds.), 1990. Water Pollution Research Reports, vol. 20. Commission of the European Communities, pp. 597–612.

Choi, J.C., Lee, M., Chun, Y., Kim, J., Oh, S., 2001. Chemical composition and source signature of spring aerosol in Seoul, Korea. Journal of Geophysical Research 106 (D16), 18,067–18,074.

Dentener, F.J., Carmichael, G.R., Zhang, Y., Lelieveld, J., Crutzen, P.J., 1996. Role of mineral aerosol as a reactive surface in the global troposphere. Journal of Geophysical Research 101, 22869–22889.

Draxler, R.R., Rolph, G.D., 2003. HYSPLIT (HYbrid Single-Particle Lagrangian Integrated Trajectory), Model Access via NOAA ARL READY Website. NOAA Air Resources Laboratory, Silver Spring, MD. http://www.arl.noaa.gov/ready/hysplit4.html.

Dulac, F., Chazette, P., 2003. Air borne study of a multi-layer aerosol structure in the eastern Mediterranean observed with the air borne polarized lidar ALEX during a STAAARTE campaign (7 June 1997). Atmospheric Chemistry and Physics 3, 1817–1831.

Escudero, M., Stein, A., Draxler, R.R., Querol, X., Alastuey, A., Castillo, S., Avila, A., 2006. Determination of the contribution of northern Africa dust source areas to $PM_{10}$ concentrations over the central Iberian Peninsula using the Hybrid Single-Particle Lagrangian Integrated Trajectory model (HYSPLIT)model. Journal of Geophysical Research 111, D06210. doi:10.1029/2005JD006395.

Gobbi, G.P., Barnaba, F., Ammannato, L., 2004. The vertical distribution of aerosols, Saharan dust and cirrus clouds in Rome (Italy) in the year 2001. Atmospheric Chemistry and Physics 4, 351–359.

Goudie, A.S., Middleton, N.J., 2001. Saharan dust storms: nature and consequences. Earth-Science Reviews 56, 179–204.

Güllü, G.H., Ölmez, I., Aygün, S., Tuncel, G., 1998. Atmospheric trace element concentrations over the Eastern Mediterranean Sea: factors affecting temporal variability. Journal of Geophysical Research 103 (D17), 21943–21954.

Guo, J., Rahn, K.A., Zhuang, G., 2004. A mechanism for the increase of pollution elements in dust storms in Beijing. Atmospheric Environment 38, 855–862.

Harrison, S.P., Kohfeld, K.E., Roelandt, C., Claquin, T., 2001. The role of dust in climate changes today, at the last glacial maximum and in the future. Earth-Science Reviews 54, 43–80.

Herman, J.R., Bhartia, P.K., Torres, O., Hsu, C., Seftor, C., Celarier, 1997. Global distribution of UV-absorbing aerosols from Nimbus 7/TOMS data. Journal of Geophysical Research 102, 16911–16922.

IPCC, 2007. Climate Change 2007. Intergovernmental Panel on Climate Change. Cambridge University Press, London.

Keyse, S., 1995. Trace Metal Chemistry of Mediterranean Rain Waters, Ph.D. Thesis. Univ. of Liverpool, UK.

Koçak, M., Nimmo, M., Kubilay, N., Herut, B., 2004. Spatio-temporal aerosol trace metal concentrations and sources in the Levantine Basin of the Eastern Mediterranean. Atmospheric Environment 38, 2133–2144.

Koçak, M., Kubilay, N., Herut, B., Nimmo, M., 2005. Dry atmospheric fluxes of trace metals (Al, Fe, Mn, Pb, Cd, Zn, Cu) over the Levantine Basin: a refined assessment. Atmospheric Environment 39, 7330–7341.

Koçak, M., Kubilay, N., Herut, B., Nimmo, M., 2007a. Trace metal solid state speciation in aerosols of the Northern Levantine Basin, East Mediterranean. Journal of Atmospheric Chemistry 56, 239–257.

Koçak, M., Mihalopoulos, N., Kubilay, N., 2007b. Chemical composition of the fine and coarse fraction of aerosols in the north Eastern Mediterranean. Atmospheric Environment 41, 7351–7368.

Krueger, B.J., Grassian, V.H., Cowin, J.P., Laskin, A., 2004. Heterogeneous chemistry of individual mineral dust particles from different dust source regions: the importance of particle mineralogy. Atmospheric Environment 38, 6253–6261.

Kubilay, N., Saydam, C., 1995. Trace elements in atmospheric particulates over the Eastern Mediterranean: concentration, sources and temporal variability. Atmospheric Environment 29, 2289–2300.

Kubilay, N., Nickovic, S., Moulin, C., Dulac, F., 2000. An illustration of the transport and deposition of mineral dust onto the Eastern Mediterranean. Atmospheric Environment 34, 1293–1303.

Kubilay, N., Çokacar, T., Oguz, T., 2003. Optical properties of mineral dust outbreaks over the northeastern Mediterranean. Journal of Geophysical Research 108 (D21), 4666. doi:10.1029/2003JD003798.

Kubilay, N., Oğuz, T., Koçak, M., Torres, O., 2005. Ground-based assessment of Total Ozone Mapping Spectrometer (TOMS) data for dust transport over the north Eastern Mediterranean. Global Biogeochemical Cycles 19, GB1022. doi:10.1029/2004GB002370.

Lelieveld, J., Berresheim, H., Borrmann, S., Crutzen, J., Dentener, F.J., Fischer, H., Feichter, J., Flatau, P.J., Heland, J., Holzinger, R., Korrmann, R., Lawrence, M.G., Levin, Z., Markowicz, K.M., Mihalopoulos, N., Minikin, A., Ramanathan, V., de Reus, M., Roelofs, G.J., Scheeren, H.A., Sciare, J., Schlager, H., Schultz, M., Siegmund, P., Steil, B., Stephanou, E.G., Stier, P., Traub, M., Warneke, C., Williams, J., Ziereis, H., 2002. Global air pollution crossroads over the Mediterranean. Science 298, 794–798.

Mamane, Y., Gottlieb, J., 1992. Nitrate formation on sea-salt and mineral particles – a single particle approach. Atmospheric Environment 26A, 1763–1769.

Mihalopoulos, N., Stephanou, E., Kanakidou, M., Pilitsidis, S., Bousquet, P., 1997. Tropospheric aerosol ionic composition in the E. Mediterranean region. Tellus 49B, 1–13.

Moulin, C., Lambert, E., Dayan, U., Masson, V., Ramonet, M., Bousquet, P., Legrand, M., Balkanski, Y.J., Guelle, W., Marticorena, B., Bergametti, G., Dulac, F., 1998. Satellite climatology of African dust transport in the Mediterranean atmosphere. Journal of Geophysical Research 103, 13137–13144.

Nickovic, S., Kallos, G., Papadopoulos, A., Kakaligpou, O., 2001. A model for prediction of desert dust cycle in the atmosphere. Journal of Geophysical Research 106, 18113–18129.

Pandolfi, M., Gonzalez-Castanedo, Y., Alastuey, A., de la Rosa, J.D., Mantilla, E., de la Campa, A.S., Querol, X., Pey, J., Amato, F., Moreno, T., 2010. Source apportionment of $PM_{10}$ and $PM_{2.5}$ at multiple sites in the strait of Gibraltar by PMF: impact of shipping emissions. Environmental Science and Pollution Research 18 (2), 260–269.

Papadimas, C.D., Hatzianastassiou, N., Mihalopoulos, N., Kanakidou, M., Katsoulis, B.D., Vardavas, I., 2009. Assessment of the MODIS Collections C005 and C004 aerosol optical depth products over the Mediterranean basin. Atmospheric Chemistry and Physics 9, 2987–2999.

Pirrone, N., Costa, P., Pacyna, J.M., 1999. Past, current and projected atmospheric emissions of trace elements in the mediterranean region. Water Science and Technology 39 (12), 1–7.

Prospero, J.M., Ginoux, P., Torres, O., Nicholson, S.E., Gill, T.E., 2002. Environmental characterization of global sources of atmospheric soil dust identified with the NIMBUS-7 total ozone mapping spectrometer. Reviews of Geophysics 40 (1), 1–31.

Putaud, J.P., Van Dingenen, R., Dell'acqua, A., Raes, F., Matta, E., Decesari, S., Facchini, M.C., Fuzzi, S., 2004. Size-segregated aerosol mass closure and chemical composition in Monte Cimone (I) during MINATROC. Atmospheric Chemistry and Physics 4, 889–902.

Querol, X., Alastuey, A., Rodriquez, S., Viana, M.M., Artinano, B., Salvador, P., Mantilla, E., Garciado Santos, S., Patier, R.F., de Las Rosa, J., Sanchez de la Campa, A., Menendez, M., Gil, J.J., 2004. Levels of particulate matter in rural, urban, and industrial sites in Spain. Science of the Total Environment 334–335, 359–376.

Rodriguez, S., Querol, X., Alastuey, A., Kallos, G., Kakaliagou, O., 2001. Saharan dust contributions to $PM_{10}$ and TSP levels in Southern and Eastern Spain. Atmospheric Environment 35, 2433–2447.

Satheesh, S.K., Moorthy, K.K., 2005. Radiative effects of natural aerosols: a review. Atmospheric Environment 39, 2089–2110.

Seguret, M.J.M., Kocak, M., Theodosi, C., Ussher, S.J., Worsfold, P.J., Herut, B., Mihalopoulos, N., Kubilay, N., Nimmo, M., 2011. Iron solubility in crustal and anthropogenic aerosols: the Eastern Mediterranean as a case study. Marine Chemistry 126 (1–4), 229–238.

Torres, O., Bhartia, B.K., Herman, J.R., Sinyuk, A., Ginoux, P., Holben, B., 2002. A long term record of aerosol optical depth from TOMS observations and comparison to AERONET measurements. Journal of Atmospheric Science 59, 398–413.

Turekian, K.K., 1976. Oceanography. Prince-Hall, Englewood Cliffs, N.J.

Underwood, G.M., Song, C.H., Phadnis, M., Carmichael, G.R., Grassian, V.H., 2001. Heterogeneous reactions of $NO_2$ and $HNO_3$ on oxides and mineral dust: a combined laboratory and modeling study. Journal of Geophysical Research 106 (D16), 18,055–18,066.

Usher, C.R., Michel, A.E., Grassin, V.H., 2003a. Reactions on mineral dust. Chemical Reviews 103, 4883–4939.

Usher, C.R., Michel, A.E., Stec, D., Grassian, V.H., 2003b. Laboratory studies of ozone uptake on processed mineral dust. Atmospheric Environment 37, 5337–5347.

Viana, M., Querol, X., Alastuey, A., Cuevas, E., Rodríguez, S., 2002. Influence of African dust on the levels of atmospheric particulates in the Canary Islands air quality network. Atmospheric Environment 36, 5861–5875.

Vrekoussis, M., Liakakou, E., Koçak, M., Kubilay, N., Oikonomou, K., Sciare, J., Mihalopoulos, N., 2005. Seasonal variability of optical properties of aerosols in the Eastern Mediterranean. Atmospheric Environment 39, 7083–7094.

Vukmirovic, Z., Unkasevic, M., Lazic, L., Tosic, I., Rajsic, S., Tasic, M., 2004. Analysis of the Saharan dust regional transport. Meteorology and Atmospheric Physics 85, 265–273.

Washington, R., Todd, M., Middleton, N.J., Goudie, Andrew S., 2003. Dust-storm source areas determined by the total ozone monitoring spectrometer and surface observations. Annals of the Association of American Geographers 93 (2), 297–313.

Wongphatarakul, V., Friedlander, S.K., Pinto, J.P., 1998. A comparative study of $PM_{2.5}$ ambient aerosol chemical databases. Environmental Science and Technology 32, 3926–3934.

Zhang, Z., Friedlander, S.K., 2000. A comparative study of chemical databases for fine particle Chinese aerosols. Environmental Science and Technology 34, 4687–4694.